Stabilization of a Swept-Wing Boundary Layer by Discrete Roughness Elements at High Reynolds Numbers

Gary Nicholson*, Lian Duan†
Missouri University of Science and Technology, Rolla, MO 65409
Mujeeb Malik‡, Fei Li§
NASA Langley Research Center, Hampton, VA 23681

Direct numerical simulations (DNS) are performed to study potential stabilizing effect of spanwise periodic discrete roughness elements (DREs) on crossflow instabilities in a spatially developing three-dimensional boundary layer over an infinite-swept natural-laminar-flow wing at a freestream Mach number of 0.75 and a chord Reynolds number of approximately 25 million. In the DNS, both the spanwise periodic DREs and distributed roughness in the leading-edge region are implemented to simulate a typical experimental scenario in which multiple steady crossflow modes including the most unstable mode (i.e., the "target" mode) emerge because of the presence of naturally distributed surface roughness in the leading edge region and spanwise periodic control cylinders of subcritical wavelength are used to force small-wavelength disturbances (i.e., the control mode) for damping the target mode. The DNS results show that the effectiveness of DRE control is sensitive to roughness diameter, height, and chordwise placement. For the DRE parameters considered in this study, the stabilizing effect on the target mode is small within the computational domain that ended at about 35% of the chord.

Nomenclature

a	speed of sound, m/s
c	unswept chord measured in direction perpendicular to leading edge, m
c_s	long, swept chord measured in direction parallel to the incoming freestream velocity, $c_s = c/\cos(\Lambda)$, m
d_r	diameter of cylindrical roughness elements, m
h_r	height of cylindrical roughness elements, m
C_p	pressure coefficient, $C_p = (p - p_\infty)/(0.5\rho_\infty Q_\infty^2)$, dimensionless
M_∞	freestream Mach number, $M_\infty = Q_\infty/a_\infty$, dimensionless
Re_c	Reynolds number based on unswept chord c, $Re_c \equiv \rho_\infty Q_\infty c/\mu_\infty$, dimensionless
Re_{c_s}	Reynolds number based on swept chord c_s, $Re_{c_s} \equiv \rho_\infty Q_\infty c_s/\mu_\infty$, dimensionless
Q_∞	free flight velocity, m/s
T	temperature, K
u	chordwise velocity, m/s
v	spanwise velocity, m/s
w	normal-to-the-chord velocity, m/s
x	Cartesian coordinate in the chordwise direction perpendicular to the leading edge of the swept wing
y	Cartesian coordinate in the spanwise direction parallel to the leading edge of the swept wing
z	Cartesian coordinate normal to the chord
i	curvilinear coordinate along the vortex axis in the nonorthogonal system

*Graduate Research Assistant. Student member, AIAA
†Assistant Professor. Senior member, AIAA
‡Senior Aerodynamicist, Computational AeroSciences Branch, M.S. 128. Fellow, AIAA
§Aerospace Technologist, Computational AeroSciences Branch, M.S. 128

j curvilinear coordinate parallel to the leading edge in the nonorthogonal system
k curvilinear coordinate defining the wall-normal direction in the nonorthogonal system
L_r spacing of the spanwise array of roughness elements, m
L_y spanwise domain size of DNS, m
A_s modal amplitude of the chordwise velocity perturbation $A_s = \max_k |\hat{u}_s|$, m/s
N logarithmic-amplification ratio, $N = \log(A_s(i)/A_s(i_0))$, dimensionless
Λ wing sweep angle, degree
β_0 fundamental disturbance spanwise wavenumber, m^{-1}

Subscripts

r quantities related to roughness
w wall variables
∞ freestream variables

Superscripts

$+$ inner wall units
$\overline{(\cdot)}$ unperturbed baseflow variables
$(\cdot)'$ perturbation from the baseflow due to roughness
$(\cdot)^*$ complex conjugate
$\hat{(\cdot)}$ spanwise Fourier transformed variables

I. Introduction

Skin-friction drag accounts for approximately one-half of the total drag for business jets and long-haul transport aircrafts. Transition delay via laminar flow technology is an important component of drag reduction technologies. Although system studies have shown that 9–10% fuel savings can be achieved by delaying boundary-layer transition over major aerodynamic surfaces, the projected benefits can be significantly offset by uncertainties in transition prediction. To enable usable and robust designs for Natural Laminar Flow (NLF) and Hybrid Laminar Flow Control (HLFC), linking transition prediction to high-fidelity aircraft design tools is critical. One important technical gap that prevents accurate transition prediction in swept-wing boundary layers is the transition due to crossflow instability, which is extremely sensitive to surface roughness, especially near the wing leading edge.[1,2]

In three-dimensional swept-wing boundary layers, crossflow instability often manifests itself in the form of stationary corotating streamwise vortices that originate at minute roughness sites. Amplitude of the induced stationary disturbances is directly related to the leading-edge surface finish. It has been found that the growth of these crossflow disturbances can be delayed by placing discrete roughness elements (DREs) of subcritical wavelengths near the wing leading edge.[3,4] Here the term subcritical refers to modes that are not critical with respect to transition. The effectiveness of the DRE concept has been demonstrated in the bulk of the existing experimental and computational studies, and these studies were carried out for low-Mach-number ($M_\infty < 0.3$) configurations with modest wing-chord Reynolds numbers of up to approximately $Re_{c_s} = 8 \times 10^6$,[1,2,5–10] and with pressure distributions that may not be optimal for wing designs for subsonic transport aircraft flying at Mach numbers between 0.75 and 0.90.

To further assess the potential capability of the DRE concept to control swept-wing transition at transonic Mach numbers and substantially higher chord Reynolds numbers than previous applications, a high-Reynolds-number flight experiment, referred to as the Subsonic Aircraft Roughness Glove Experiment (SARGE), was recently initiated to design high-Reynolds-number NLF wing configurations with the maximum possible chord Reynolds number approaching $Re_{c_s} = 30 \times 10^6$.[11] For such configurations, Malik et al.[12] and Li et al.[13] conducted a computational assessment of the DRE concept using nonlinear parabolized stability equations (PSE) and secondary-instability analysis. The particular conditions used for this assessment consisted of a freestream Mach number of 0.75 and chord Reynolds numbers of 17×10^6, 24×10^6, and 30×10^6. The computations demonstrated that DREs can suppress dominant boundary-layer disturbances at the chosen Reynolds numbers. However, in their calculations, the receptivity phase was not incorporated. Instead, a linear eigenmode was used to initialize the calculation while the impact of the actual surface roughness to initiate natural crossflow disturbances, as well as the control mode, was not simulated. Given that it is not known how far downstream of the DREs a crossflow eigenmode shape develops and what the relation of its amplitude to the height and shape of the roughness is, a further study of receptivity to rough-

ness (i.e., the relation between the size and/or distribution of roughness and induced stationary disturbance in the boundary-layer) is needed for a given DRE height, shape, and location in order to draw definitive conclusions on whether DREs can delay crossflow-induced transition.

Direct numerical simulation (DNS) is a valuable tool that can be combined with stability analysis to estimate the range of amplitudes of the stationary-crossflow instabilities excited by surface roughness. DNS can be used to elucidate features of roughness-induced flow fields[7,8,10,14,15] and validate reduced-order receptivity models such as those based on PSE[16] and linearized Navier-Stokes equations.[17,18] Most of the previous studies were carried out for low-Mach-number configurations with modest wing-chord Reynolds numbers, and these studies concluded that DREs stabilize the primary crossflow modes and attenuate the growth of secondary instabilities. To provide computational assessment of the DRE technology for potential application to transport aircraft, the current authors[19] performed DNS of receptivity to roughness for a swept-wing configuration (G-IIB, TAMU-0706 wing glove) at a freestream Mach number of 0.75 and a chord Reynolds number of approximately 25 million based on the long, swept chord. Either critically spaced discrete cylinders of micron size or naturally occurring distributed roughness in the leading-edge region were applied to excite stationary crossflow disturbances. The DNS data showed that the spanwise spectral content of the excited crossflow disturbances is highly dependent upon the shape of roughness elements, and the initial growth of the crossflow structures is a nonlinear function of the element height. The nonlinear dependence of the initial amplitude of the excited crossflow disturbances on roughness height is consistent with the finding by Kurz and Kloker[15] at a freestream Mach number of 0.65 and a chord Reynolds number of approximately 10 million. Additionally, the linear growth rate of the excited crossflow disturbances predicted by DNS shows good agreement with linear PSE.

As a follow up to the receptivity study by Nicholson et al.[19] at transport-relevant Reynolds numbers, the current paper studies the stabilization of the naturally most unstable steady crossflow mode by spanwise periodic DREs using direct numerical simulation (DNS) of compressible Navier-Stokes equations over a realistic NLF wing configuration at Reynolds numbers relevant to transport aircraft. DNS results are analyzed to determine the effectiveness and robustness of DREs in attenuating the naturally most unstable steady crossflow mode at the choosen high Reynolds number.

The paper is structured as follows. The flow conditions and numerical methods are outlined in Section II. Section III presents DNS results of stabilization of crossflow instabilities with DREs of subcritical wavelengths over a realistic NLF wing configuration at a Reynolds number relevant to transport aircraft. Section IV gives a summary of the current study.

II. Flow Conditions and Numerical Methodology

The work in this paper considers the boundary layer over a swept NLF wing (G-IIB, TAMU-0706 wing glove) designed by Tufts et al.[20] at Texas A & M University. The design of the TAMU-0706 wing glove is an improvement to that of Belisle et al.[11] with a truly uniform flow in the spanwise direction and substantially improved stability characteristics. The target design conditions consist of $M_\infty = 0.75$ at an altitude of $H = 40$ kft, an angle of attack (AoA) of 3.7 degrees, a chord Reynolds number, Re_{c_s}, of 24.77 million, and a leading-edge sweep angle, Λ, of 30°. The free flight conditions for the work described in this paper are summarized in Table 1. In this paper, we focus on an infinite-swept TAMU-0706 wing at an AoA of 1.9375 degrees. For the selected angle of attack, the surface pressure coefficient C_p near the leading edge of the infinite-swept wing matches as closely as possible that of the three-dimensional (3-D) finite-swept counterpart at the design AoA of 3.7 degrees.[19]

Table 1. Free flight conditions for the DNS.

M_∞	Q_∞ (m/s)	ρ_∞ (kg/m^3)	T_∞ (K)	c (m)	$Re_c(\times 10^6)$	$Re_{c_s}(\times 10^6)$
0.75	221.28	0.302	216.65	3.83	21.45	24.77

For the selected configuration, two sets of DNS are carried out. A DNS without roughness, referred to as DNS-I, is first computed to simulate the steady baseflow that serves to provide freestream and outlet

boundary conditions for a second DNS that includes roughness, referred to as DNS-II. To select a suitable domain for DNS-I, a precursor Reynolds-averaged Navier-Stokes (RANS) simulation of the flow for the entire wing is carried out and the flowfield is explored. In the RANS computations, the Spalart-Allmaras turbulence model is used; and the flow is assumed to be homogeneous in the spanwise direction. The flow is set to be laminar over the first 61% of the wing on both the upper and lower surfaces and the turbulence model is only switched on outside of the laminar region. In DNS-II, surface roughness is incorporated to excite crossflow disturbances. The roughness elements implemented in the DNS include a strip of distributed roughness that is modeled by inhomogeneous boundary conditions from projecting the no-slip condition at the undisturbed wall and a spanwise periodic row of discrete circular cylinders of various spacing and diameters that is formed by displacing the corresponding mesh points at the wall (see Section III). The distributed roughness mimics that in the leading edge region of an experimental wing, the presence of which stimulates multiple steady crossflow modes including the naturally most unstable mode (i.e., the "target" mode). The circular cylinders are introduced to excite the subcritical crossflow mode (i.e, the "control" mode) for damping the target mode.

The wing and the adopted coordinate systems are shown in Figure 1. A nonorthogonal coordinate system is used for the current DNS. In this coordinate system, the body-fitted curvilinear computational coordinate i is approximately aligned with the crossflow vortex axis rather than along the chordwise direction (x direction). By doing so, the number of grid points, which is required in the streamwise direction due to the relatively slow evolution of crossflow modes along this direction, can be substantially reduced. The spanwise computational coordinate j is along the y direction, which is parallel to the leading edge of the wing and at an acute angle to the i-coordinate. Similar nonorthogonal systems have been chosen in spatially developing secondary instability analyses[21] and DNS[22,23] for crossflow-dominated swept-wing boundary layers. Both DNS-I and DNS-II simulate the physical boundary layer over the TAMU wing extending approximately from $x/c = 0.006$ on the wing lower surface or windward side to $x/c = 0.7$ on the wing upper surface or leeward side. Only the flow field on the leeward side is of interest, while part of the windward side is retained to account for the asymmetry of the configuration. Negligible differences have been observed when the domain is further enlarged on the wing lower surface. The DNS domain size in the spanwise direction is chosen such that both the naturally most unstable mode and the control mode can be accounted for. The spanwise domain was chosen to be 17 mm, as the study of receptivity to surface roughness has identified that the wavelength of the naturally most unstable stationary crossflow mode is 8.5 mm for this specific NLF wing configuration.[19] Sponge regions are inserted in both types of DNS in order to minimize acoustic reflections at the lower and upper outlets and at the freestream boundary (Figure 2). Within these sponge regions, the flow is forced toward the RANS solution for the entire TAMU wing. On the wall, no-slip conditions are applied for the three velocity components and the wall temperature extracted from the RANS solution (in which an adiabatic condition is used) is prescribed as Dirichlet conditions in the DNS.

To simulate the boundary layer flow over the domain, the compressible Navier-Stokes equations are solved in generalized curvilinear coordinates. The working fluid is assumed to be an ideal gas with a linear (i.e., Newtonian) stress-strain relation. The Fourier law is used to compute the heat flux terms. A 7th-order weighted essentially nonoscillatory (WENO) scheme[24] is used to compute the convective flux terms. Given the subsonic nature of the flow without shock waves, the optimal 9-point WENO stencil is used in the simulations with WENO adaptation turned off to reduce numerical dissipation. For the viscous flux terms, a 4th-order central difference scheme is used. The 3rd-order low-storage Runge-Kutta scheme by Williamson[25] is used for time integration. Additional details of the numerical methodology are given in Nicholson et al.[19] In particular, the validity of the baseflow computed by the DNS is checked by comparing DNS-I that consists of a partial wing with the full-wing RANS. Excellent comparison between the RANS and the DNS has been achieved.[19] For DNS-II, the total number of grid points is 4949, 640, and 295 in the streamwise (i), spanwise (j), and wall-normal (k) directions, respectively. The computational grid resolution is comparable to that reported in Nicholson et al.[19]

III. Results

In this section, subcritical DRE control in the swept TAMU-0706 wing at $Re_{c_s} = 24.77$ million is investigated by studying its effect on primary stationary crossflow disturbances. Two cases are considered. First, DNS without DRE control is conducted using the distributed natural roughness model only to show the effectiveness of the natural distributed roughness in exciting the multiple steady crossflow modes including

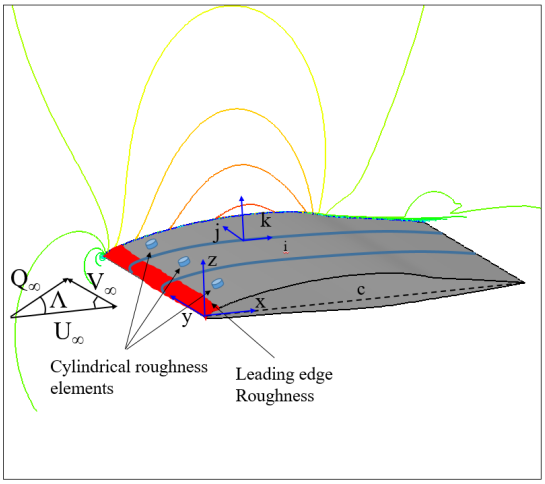

Figure 1. Swept TAMU-0706 wing, with sweep angle $\Lambda = 30^\circ$ and the total incoming velocity Q_∞. The wing is at an angle-of-attack of 1.9375°. Here, (i, j, k) and (x, y, z) represent locally fitting curvilinear and Cartesian coordinate systems, respectively. The colored contours denote the chordwise velocity ($\overline{u}$) from the RANS. The blue lines represent the crossflow vortex axis.

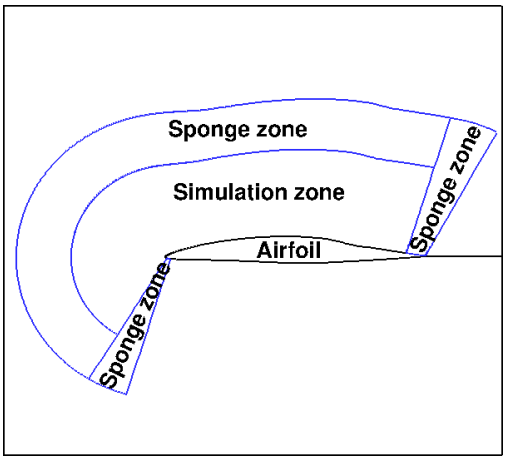

Figure 2. Sketch of the computational domain and boundary conditions for the DNS simulation.

the naturally most unstable mode (i.e., the "target" mode). Next, DNS are performed comprising both the natural and the control roughness to simulate a typical experiment scenario in which multiple steady crossflow modes including the most unstable mode emerge because of the presence of naturally distributed surface roughness in the leading edge region and spanwise periodic control cylinders of subcritical wavelength are used to force small-wavelength disturbances (i.e., the "control" mode) for damping the target mode. The DNS without and with DRE control are denoted as the "natural" and the "controlled" cases, respectively, in the rest of the paper.

A. Receptivity to Distributed Natural Surface Roughness

First, the emergence of unstable crossflow modes due to the presence of natural surface roughness in the leading edge region is computed by DNS. We simulate the effect of natural surface roughness following a procedure proposed by Hosseini et al.,[10] in which roughness is modeled by covering the leading-edge region of the infinite-swept wing with a spanwise periodic roughness strip of the form

$$h_r(x,y) = \epsilon_r H_\beta(x) \sum_{n=1}^{MN} \sin(n\beta_0 y + \varphi_n), \qquad \text{with} \quad \beta_0 = 2\pi/L_y, \quad H_\beta(x) = \left[S\left(\frac{x-x_s}{L_1}\right) - S\left(\frac{x-x_e}{L_2}+1\right)\right]. \tag{1}$$

Here h_r denotes the wall-normal displacement whose magnitude can be adjusted with the value of ϵ_r; β_0 and L_y is the fundamental spanwise wavenumber and spanwise DNS domain size, respectively; x_s and x_e denote the starting and ending chordwise locations of the roughness strip, respectively; L_1 and L_2 is the length of the smoothing zone at the start and end of the roughness, respectively; S is a smooth step function defined in Schrader et al.;[26] and φ_n is the modal phase chosen randomly. Because of the spanwise periodic boundary conditions, only disturbances with a wavenumber of $n\beta_0$ (n = 1, 2, ...) can be accounted for in the DNS. Figure 3 provides a schematic of the model parameters. The roughness model, referred to in this paper as "natural" surface roughness, is implemented as inhomogeneous boundary conditions by projecting the no-slip conditions on the surface of the roughness to the undisturbed wall using Taylor-series expansions as[27]

$$\begin{aligned} u|_w &= -h_r \left(\left.\frac{\partial \overline{u}}{\partial n}\right|_w \right) \\ v|_w &= -h_r \left(\left.\frac{\partial \overline{v}}{\partial n}\right|_w \right) \\ w|_w &= -h_r \left(\left.\frac{\partial \overline{w}}{\partial n}\right|_w \right) \\ T|_w &= \overline{T}|_w - h_r \left(\left.\frac{\partial \overline{T}}{\partial n}\right|_w \right). \end{aligned} \tag{2}$$

Table 2 lists the values of the model parameters for the DNS of the natural case. The roughness parameters are determined based on the lessons learned from the previous study of receptivity to surface roughness for the same swept-wing configuration as reported by Nicholson et al.[19] In particular, the value of ϵ_r is similar to the r.m.s. natural roughness height of highly polished aluminum surfaces,[28] with the ratio of the roughness height to the local boundary-layer thickness $\epsilon_r/\delta \approx 0.02\%$.

Figure 4a shows the chordwise evolution of disturbance amplitudes A_s normalized by Q_∞ for the natural DNS case (Case NatH0p1), while Figure 4b shows the logarithmic-amplification ratios N. The natural roughness elements are effective in exciting a wide spectrum of spanwise modes. As expected from the previous receptivity study,[19] the 8.5-mm mode becomes dominant over all the smaller wavelength modes after $x/c = 0.3$ and remains unstable over longer streamwise distances, while all the smaller wavelength modes grow first (i.e., at small distance from the wing leading edge) but decay farther downstream. Among all the subcritical modes, the 5.67-mm mode ($3\beta_0$) experiences strong initial growth (with a maximum N factor of approximately 6) and the initial amplitudes is maintained over a relatively large streamwise distance up to $x/c \approx 0.42$.

Table 2. Summary of roughness parameters for DNS study of receptivity to distributed natural surface roughness.

Case	ϵ_r (μm)	L_y (mm)	MN	x_s/c	x_e/c	L_1/c	L_2/c
NatH0p1	0.1	17	10	-0.854%	0.131%	1.31×10^{-3}	2.61×10^{-4}

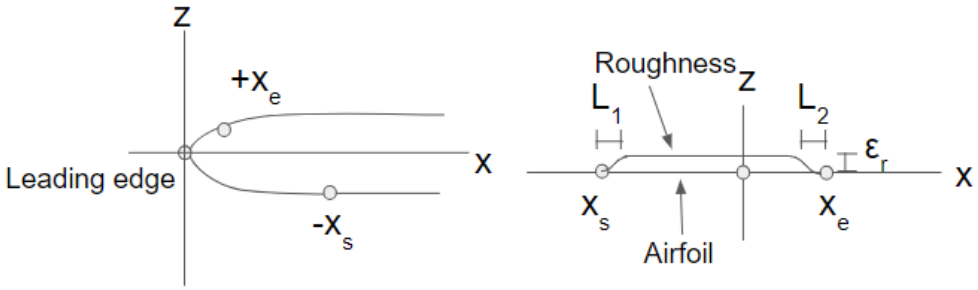

Figure 3. Schematic of the model parameters for natural roughness used in the DNS.

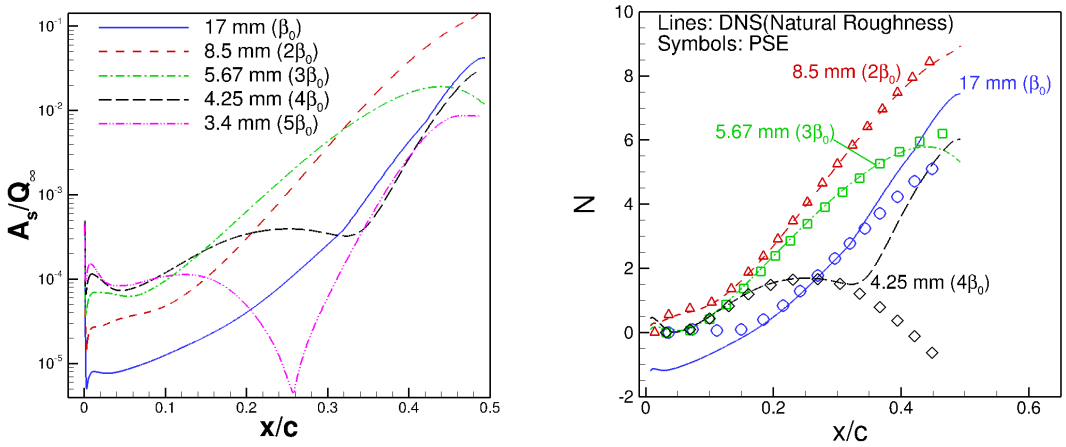

(a) (b)

Figure 4. (a) Normalized modal amplitude A_s/Q_∞ and (b) logarithmic-amplification ratios N as predicted by DNS for the natural case (Case NatH0p1).

B. Control of Crossflow Instabilities with DREs of Subcritical Wavelengths

Next, the control of the naturally most unstable steady crossflow mode is investigated using DNS that implement both natural roughness that stimulates multiple steady crossflow modes, including the naturally most unstable mode and control cylinders that excite subcritical crossflow disturbances. In the DNS, the naturally distributed roughness is modeled with the roughness model of Eq. 1 whose parameters are listed in Table 2, while the control cylinders are inserted by displacing the corresponding meshes at the wall using the parameters listed in Table 3. The spacing of control cylinders L_r is selected to be 2/3 of the wavelength of the naturally most unstable steady crossflow mode (i.e., the 8.5-mm mode), given that the DNS for the natural case (Case NatH0p1), as well as the PSE, has confirmed that the 5.67-mm mode experiences a strong initial growth with a logarithmic-amplification ratio N as large as 5 but decay farther downstream (Figure 4). The selection of control cylinders with a spanwise spacing of 2/3 of the wavelength of the target mode is consistent with earlier experiments[3,4] and a recent DNS that simulated crossflow control with DREs over a low-speed swept wing at $Re_{c_s} = 2.4 \times 10^6$.[10] The roughness diameter d_r, height h_r, and chordwise placement x_r/c are varied to determine how the initial spanwise content of the roughness-induced perturbations depends on these parameters.

Table 3. Overview of DNS cases for studying the control of crossflow instabilities with cylindrical surface roughness together with the respective roughness parameters.

Case	Location x_r/c	Diameter d_r (mm)	Height h_r (μm)	Spacing L_r (mm)
Ctl_D2p0_H20_L5p67	0.0027	2.0	20	5.67
Ctl_D3p0_H20_L5p67	0.0027	3.0	20	5.67
Ctl_D3p7_H20_L5p67	0.0027	3.7	20	5.67
Ctl_D4p25_H20_L5p67	0.0027	4.25	20	5.67
Ctl_D4p6_H20_L5p67	0.0027	4.6	20	5.67
Ctl_D3p7_H10_L5p67	0.0027	3.7	10	5.67
Ctl_D3p7_H30_L5p67	0.0027	3.7	30	5.67
Ctl_D3p7_H20_L5p67_xc1p5	0.015	3.7	20	5.67

1. *Effect of Diameter*

To determine how the initial spanwise content of the roughness-induced perturbations depends on roughness diameter, DRE control is simulated for control cylinders with five different diameters (d_r = 2.0 mm, 3.0 mm, 3.7 mm, 4.25 mm, and 4.6 mm). The diameter values range from 35% to 81% of the spanwise roughness spacing L_r (i.e., $35\% \leq d_r/L_r \leq 81\%$). Figure 5 shows the chordwise evolution of disturbance amplitudes A_s/Q_∞ for the controlled cases with different diameters. For all the cases, the diameter of control cylinders has a negligible influence on large-wavelength disturbances (i.e., disturbances with a wavelength larger than the roughness spacing L_r), while it has a large impact on the modal amplitude of the control mode (5.67-mm mode), which has a wavelength equal to the roughness spacing. Such a trend is consistent with the experiment by Saric et al.[4] who observed that only the mode with wavelength equal to the DRE spacing and its superharmonics are excited by DREs. A comparison in the initial spanwise wavenumber spectra among the cases with different diameters (Figure 5f) shows that the modal amplitude of the control mode ($3\beta_0$) increases nonlinearly with the cylinder diameter. Cylinder diameter has a large impact on the modal amplitude of the control mode up to at least $d_r \approx 3.7$ mm or $d_r/L_r \approx 65\%$. At larger diameters, the influence of diameter continues largely for the superharmonics of the control mode $3\beta_0$, as opposed to the control mode itself, and minimal increases occur for the control mode (Figure 6).

2. *Effect of Roughness Height*

The effect of roughness height on the initial spanwise content of roughness induced perturbations is studied by varying the height of DREs, between 10 μm and 30 μm, with a fixed roughness diameter of $d_r = 3.7$ mm and chordwise placement of $x_r/c = 0.0027$. The selected values of roughness height h_r range from 2–6%

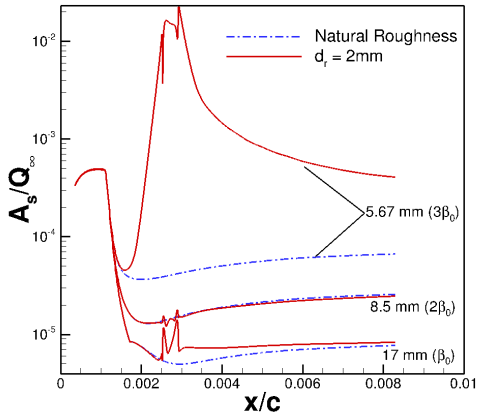

(a) $d_r = 2.0$ **mm,** $d_r/L_r = 35\%$

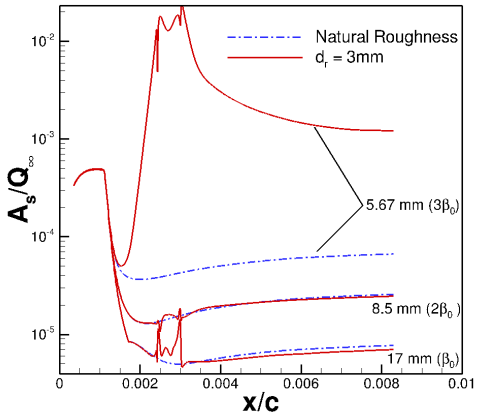

(b) $d_r = 3.0$ **mm,** $d_r/L_r = 53\%$

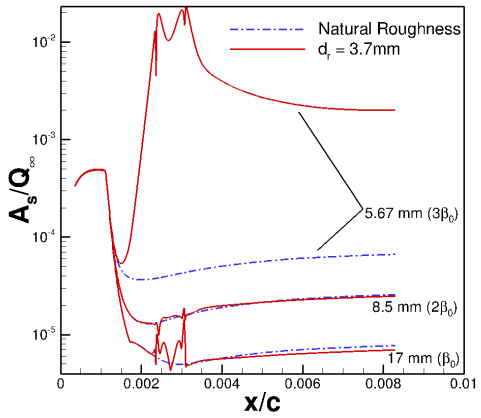

(c) $d_r = 3.7$ **mm,** $d_r/L_r = 65\%$

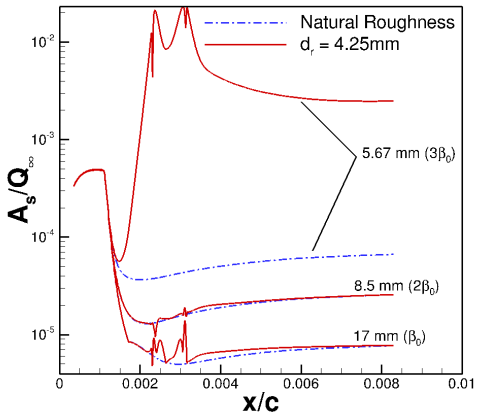

(d) $d_r = 4.25$ **mm,** $d_r/L_r = 75\%$

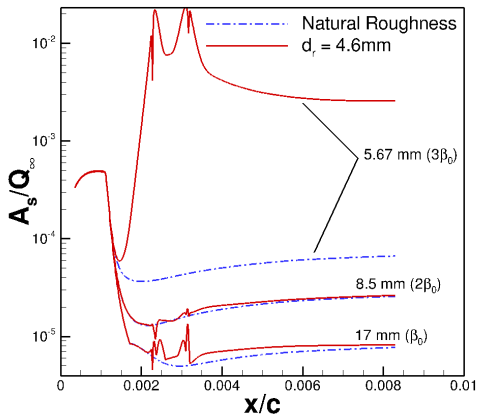

(e) $d_r = 4.6$ **mm,** $d_r/L_r = 81\%$

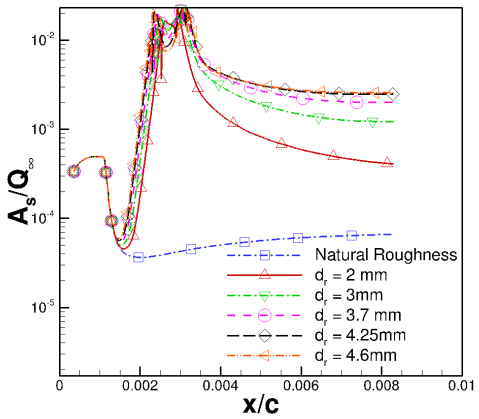

(f) **Comparison of the** $3\beta_0$ **mode**

Figure 5. Chordwise evolution of normalized disturbance amplitudes A_s/Q_∞ of the fundamental mode β_0 (17-mm mode) and the first two superhamonics ($2\beta_0$, $3\beta_0$) as predicted by DNS for the controlled cases with varying diameters. (a) Case Ctl_D2p0_H20_L5p67; (b) Case Ctl_D3p0_H20_L5p67; (c) Case Ctl_D3p7_H20_L5p67; (d) Case Ctl_D4p25_H20_L5p67; (e) Case Ctl_D4p6_H20_L5p67; (f) Comparison in A_s/Q_∞ of $3\beta_0$ (5.67-mm) mode among the controlled cases with varying diameters.

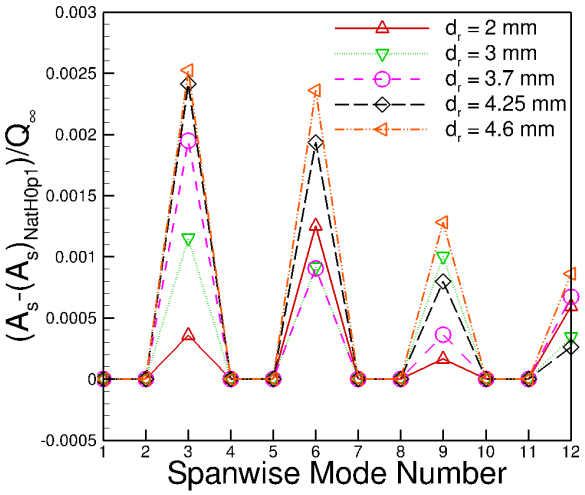

Figure 6. Comparison in spanwise wavenumber spectra at $x/c = 0.008$ among the controlled cases with varying diameters (Cases Ctl_D2p0_H20_L5p67, Ctl_D3p0_H20_L5p67, Ctl_D3p7_H20_L5p67, Ctl_D4p25_H20_L5p67, and Ctl_D4p6_H20_L5p67).

of the local boundary-layer thickness. Figure 7 shows the chordwise evolution of disturbance amplitudes A_s/Q_∞ for the controlled cases with different heights (Cases Ctl_D3p7_H10_L5p67, Ctl_D3p7_H20_L5p67, Ctl_D3p7_H30_L5p67). The primary change caused by increasing roughness height is an increase in the amplitude of the control mode and its superharmonics. The dependence of initial disturbance amplitude on roughness height is nonlinear, with the amplitude of the control mode for the case with $h_r = 30$ μm being 3.5 times larger than that for the case with $h_r = 10$ μm. Such a nonlinear dependence on roughness height is consistent with the previous study of receptivity to cylindrical roughness[19] and the findings by Kurz and Kloker[15] who noted a superlinear dependence of the roughness height on disturbance amplitude. In contrast to roughness diameter that is found to influence both the amplitude and modal content of the excited crossflow modes, Figure 8 suggests that roughness height has little influence on the relative spanwise content.

3. Effect of Chordwise Placement

The dependence of roughness-induced crossflow disturbances on the chordwise location of control cylinders (x_r/c) is studied by comparing DRE controls with control cylinders placed at $x_r/c = 0.0027$ (Case Ctl_D3p7_H20_L5p67) and $x_r/c = 0.015$ (Case Ctl_D3p7_H20_L5p67_xc1p5). $x_r/c = 0.0027$ corresponds approximately to the neutral point of the naturally most unstable crossflow mode (i.e., the 8.5-mm mode) while $x_r/c = 0.015$ is farther downstream of the neutral point after most of the naturally occurring crossflow modes undergo initial growth (see Figure 4a). Figure 9a shows normalized disturbance amplitudes A_s/Q_∞ of the fundamental mode β_0 (17-mm mode) and the first two superhamonics ($2\beta_0$, $3\beta_0$) as predicted by DNS for the two controlled cases. Consistent with the observation by Saric et al.,[4] the chordwise placement of control cylinders has a negligible influence on disturbances with a wavelength larger than the roughness spacing L_r, while it has a significant impact on the modal amplitude of the control mode (5.67-mm mode), which has a wavelength equal to the roughness spacing. DREs are significantly more effective in stimulating the control mode if they are placed closer to the neutral point of the most unstable mode, as seen in Figure 9b where the increase in the amplitude of the control mode is nearly twice for the case with DREs placed closer to the neutral point. The finding confirms previous observations that it would be easier for DREs to excite the control mode before such a mode has grown significantly.[2,4] This in turn has an effect on the effectiveness of the DREs in damping the most unstable mode ($2\beta_0$) as can be seen in Figure 9c where the $2\beta_0$ mode has begun to grow more slowly around $x/c = 25\%$ for the case with DREs placed at the neutral point (Ctl_D3p7_H20_L5p67) but has shown minimal decay even up to $x/c = 38\%$ for the case with DREs placed farther downstream(Ctl_D3p7_H20_L5p67_xc1p5). Figure 9c further shows that there is small stabi-

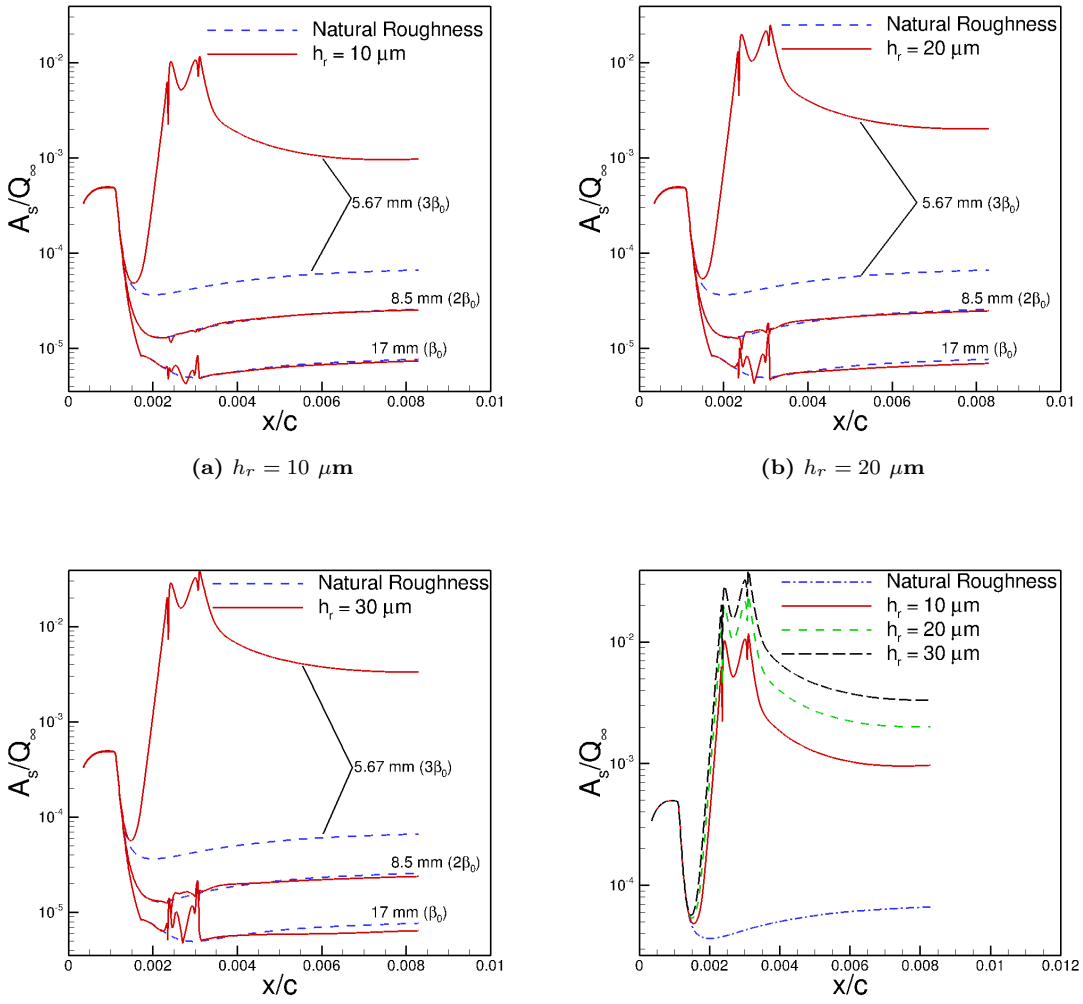

(a) $h_r = 10$ μ**m**

(b) $h_r = 20$ μ**m**

(c) $h_r = 30$ μ**m**

(d) Comparison of the $3\beta_0$ **mode**

Figure 7. Chordwise evolution of normalized disturbance amplitudes A_s/Q_∞ **of the fundamental mode** β_0 **(17-mm mode) and the first two superhamonics (**$2\beta_0$**,** $3\beta_0$**) as predicted by DNS for the controlled cases with varying heights. (a) Case Ctl_D3p7_H10_L5p67; (b) Case Ctl_D3p7_H20_L5p67; (c) Case Ctl_D3p7_H30_L5p67; (d) Comparison in** A_s/Q_∞ **of** $3\beta_0$ **(5.67-mm mode) among the controlled cases with varying heights.**

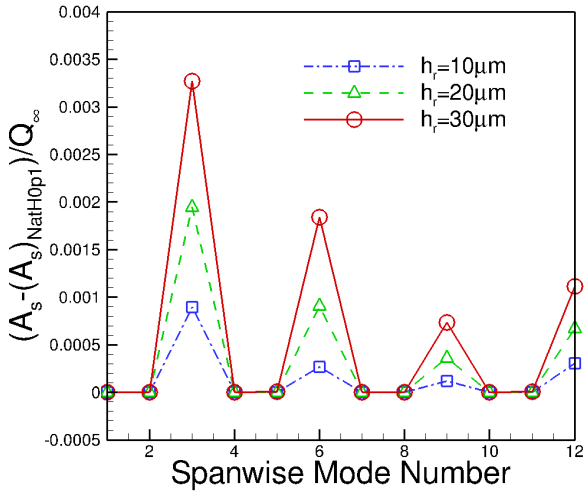

Figure 8. Comparison in spanwise wavenumber spectra at $x/c = 0.008$ among the controlled cases with varying heights (Cases Ctl_D3p7_H10_L5p67, Ctl_D3p7_H20_L5p67, and Ctl_D3p7_H30_L5p67).

lizing effect on the target mode ($2\beta_0$ mode) up to $x/c = 35\%$ for the case with DREs placed at the neutral point (Case Ctl_D3p7_H20_L5p67). Hosseini et al.[10] reported that DREs do not cause significant reduction in the amplitude of the target mode until $40\% < x/c < 50\%$ for a low-speed swept-wing configuration at $Re_{c_s} = 2.4 \times 10^6$. Further simulations that track the crossflow disturbances farther downstream are necessary to see if a similarly significant stabilization occurs for the current swept wing at a significantly higher chord Reynolds number.

IV. Summary

Direct numerical simulations (DNS) are conducted to study the potential stabilizing effect of spanwise periodic DREs on crossflow instabilities in the transonic TAMU-0706 wing glove boundary layer at a high wing-chord Reynolds number in the absence of unsteady perturbations. The surface roughness implemented in the DNS includes discrete meshed cylinders combined with cyclic boundary conditions, which mimics a spanwise periodic row of roughness elements, and an appropriate simplified roughness model combined with inhomogeneous boundary conditions at the undisturbed wall, which mimics naturally occurring distributed roughness. The spacing of the control cylinders is chosen to be 2/3 of the wavelength of the naturally most unstable disturbance so as to excite steady crossflow disturbances that are subcritical with respect to transition. Roughness parameters including the diameter, height, and streamwise placement of the control cylinders are varied in the DNS to show the effectiveness and robustness of DREs in exciting the control mode for attenuating the naturally most unstable steady crossflow mode. The DNS for the natural case (i.e., using the distributed natural roughness model only) shows that the natural roughness elements can excite a wide spectrum of spanwise modes including the naturally most unstable mode; the linear growth of the excited unstable crossflow disturbances predicted by DNS shows good agreement with linear PSE. The DNS for the controlled cases show that the excitation of subcritical modes is sensitive to the diameter, chordwise placement, and spanwise spacing of the DREs. In order to most effectively force the control mode, DREs need to have a diameter of at least 2/3 of the roughness spacing, have large enough height (up to at least 6% of the local boundary-layer thickness), and be placed in the immediate vicinity of the neutral point of the most unstable mode. For the parameters considered in this study, there is only a small stabilizing effect on the target mode up to $x/c = 35\%$. Further study that tracks the crossflow modes farther downstream is necessary to demonstrate whether the stabilizing effect becomes larger at $x/c > 35\%$ and whether DRE control would cause a significant delay in transition for the selected flight-relevant flow conditions.

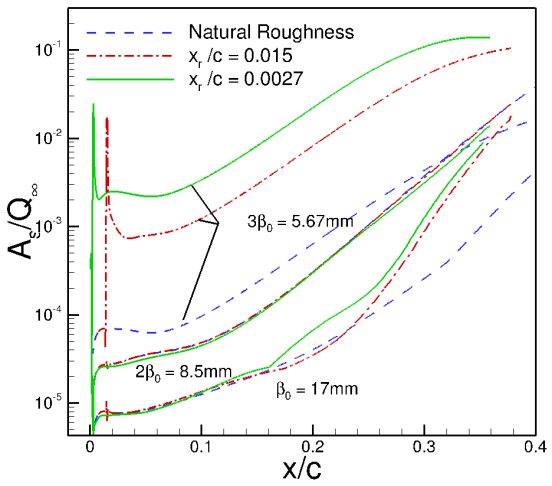

(a) Chordwise evolution of A_s/Q_∞

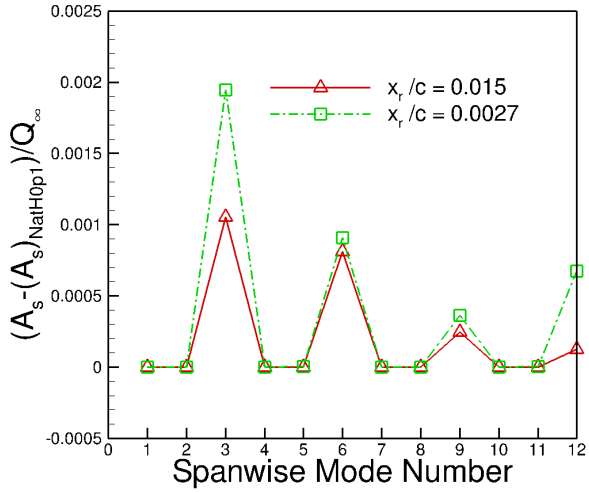

(b) Initial spanwise wavenumber spectra

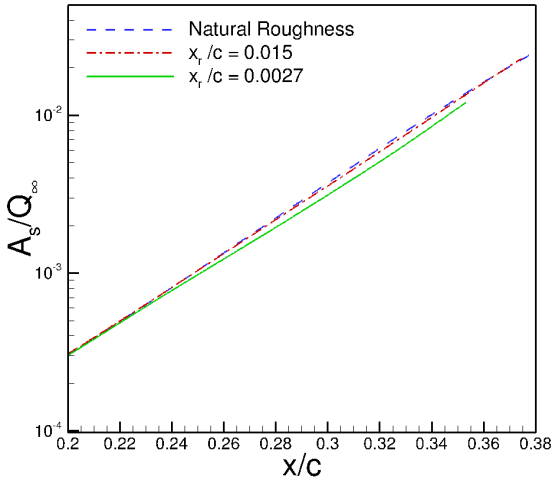

(c) Zoomed-in view of $2\beta_0$ mode

Figure 9. Comparison in disturbance amplitudes and spnwise wavenumber spectra among the controlled cases with varied chordwise placement x_r/c (Cases Ctl_D3p7_H20_L5p67 and Ctl_D3p7_H20_L5p67_x1p5); (a) Chordwise evolution of A_s/Q_∞ of the fundamental mode β_0 (17-mm mode) and the first two superhamonics ($2\beta_0$, $3\beta_0$); (b) initial spanwise wavenumber spectra at $(x - x_r)/c = 0.0053$ (approximately $5.5d_r$ downstream from the DREs); (c) zoomed-in view of A_s/Q_∞ for the target mode (i.e., 8.5-mm mode) near region of damped growth.

Acknowledgments

This work was originally sponsored under the NASA Environmentally Responsible Aviation Project.

References

[1]Carpenter, A. L., Saric, W. S., Reed, H. L., and Saric, W. S., "Laminar Flow Control on a Swept Wing with Distributed Roughness," AIAA Paper 2008-7335, 2008.

[2]Saric, W. S., Carpenter, A. L., and Reed, H. L., "Passive Control of Transition in Three-Dimensional Boundary Layers, with Emphasis on Discrete Roughness Element," *Phil. Trans. R. Soc. A*, Vol. 369, No. 1940, 2011, pp. 1352–1364.

[3]Saric, W. S., Carrillo, R. B., and Reibert, M. S., "Nonlinear Stability and Transition in 3-D Boundary Layers," *Meccanica*, Vol. 33, 1998, pp. 469–487.

[4]Saric, W. S., Carrillo, R. B., and Reibert, M. S., "Leading-edge Roughness as a Transition Control Mechanism," AIAA Paper 1998-0781, 1998.

[5]Malik, M. R., Li, F., Choudhari, M. M., and Chang, C. L., "Secondary Instability of Crossflow Vortices and Swept-Wing Boundary-Layer Transition," *Journal of Fluid Mechanics*, Vol. 399, 1999, pp. 85–115.

[6]Haynes, T. S. and Reed, H. L., "Simulation of Swept-Wing Vortices using Nonlinear Parabolized Stability Equations," *Journal of Fluid Mechanics*, Vol. 405, 2000, pp. 325–349.

[7]Wassermann, P. and Kloker, M., "Mechanisms and Passive Control of Crossflow-Vortex-Induced Transition in a Three-Dimensional Boundary Layer," *Journal of Fluid Mechanics*, Vol. 456, 2002, pp. 49–84.

[8]Rizzetta, D. P., Visbal, M. R., Reed, H. L., and Saric, W. S., "Direct Numerical Simulation of Discrete Roughness on a Swept-Wing Leading Edge," *AIAA Journal*, Vol. 48, No. 11, 2010, pp. 2660–2673.

[9]Li, F., Choudhari, M. M., Chang, C.-L., Streett, C., and Carpenter, M., "Computational Study of Laminar Flow Control on a Subsonic Swept Wing Using Discrete Roughness Elements," *AIAA Journal*, Vol. 49, No. 3, 2011, pp. 520–529.

[10]Hosseini, S. M., Tempelmann, D., Hanifi, A., and Henningson, D. S., "Stabilization of a Swept-Wing Boundary Layer by Distributed Roughness Elements," *Journal of Fluid Mechanics*, Vol. 718, 2013, pp. R1–R11.

[11]Belisle, M. J., Roberts, M. W., Tufts, M. W., Tucker, A. A., Williams, T., Saric, W. S., and Reed, H. L., "Design of the Subsonic Aircraft Roughness Glove Experiment (SARGE)," AIAA Paper 2011-3524, 2011.

[12]Malik, M., Liao, W., Li, F., and Choudhari, M., "Discrete-Roughness-Element-Enhanced Swept-Wing Natural Laminar Flow at High Reynolds Numbers," *AIAA Journal*, Vol. 53, No. 8, 2015, pp. 2321–2334.

[13]Li, F., Choudhari, M. M., Carpenter, M., Malik, M., Chang, C.-L., and Streett, C., "Control of Crossflow Transition at High Reynolds Numbers Using Discrete Roughness Elements," *AIAA Journal*, Vol. 54, No. 1, 2016, pp. 39–52.

[14]Piot, E., Content, C., and Casalis, G., "Receptivity of Crossflow Instabilities to a Periodic Roughness Array on a Swept Cylinder: Investigation of the Roughness Size Influence," AIAA Paper 2008-0502, 2008.

[15]Kurz, H. B. E. and Kloker, M. J., "Receptivity of a Swept-Wing Boundary Layer to Micro-sized Discrete Roughness Elements," *Journal of Fluid Mechanics*, Vol. 755, 2014, pp. 62–82.

[16]Tempelmann, D., Schrader, L. U., Hanifi, A., Brandt, L., and Henningson, D. S., "Swept Wing Boundary-Layer Receptivity to Localized Surface Roughness," *Journal of Fluid Mechanics*, Vol. 711, 2012, pp. 516–544.

[17]Collis, S. S. and Lele, S. K., "Receptivity to Surface Roughness Near a Swept Leading Edge," *Journal of Fluid Mechanics*, Vol. 380, 1999, pp. 141–168.

[18]Thomas, C., Mughal, S., and Ashworth, R., "On Predicting Receptivity to Surface Roughness in a Compressible Infinite Swept Wing Boundary Layer," *Physics of Fluids*, Vol. 29, No. 3, 2017, pp. 034102.

[19]Nicholson, G. L., Zhang, C., Duan, L., Malik, M. R., Li, F., and Uzun, A., "Direct Numerical Simulation of Receptivity to Roughness in a Swept-Wing Boundary Layer at High Reynolds Numbers," AIAA Paper 2018-3076, 2018.

[20]Tufts, M. W., Reed, H. L., and Saric, W. S., "Design of an Infinite-Swept-Wing Glove for In-Flight Discrete-Roughness-Element Experiment," *Journal of Aircraft*, Vol. 51, No. 5, 2014, pp. 1618–1631.

[21]Li, F. and Choudhari, M. M., "Spatially Developing Secondary Instabilities and Attachment Line Instability in Supersonic Boundary Layers," AIAA Paper 2008-590, 2008.

[22]Jiang, L., Choudhari, M. M., Chang, C. L., and Liu, C., "Direct Numerical Simulations of Crossflow Disturbances in Supersonic Boundary Layers," AIAA Paper 2004-589, 2004.

[23]Duan, L., Choudhari, M. M., and Li, F., "Direct Numerical Simulation of Transition in a Swept Boundary Layer," AIAA Paper 2013-2617, 2013.

[24]Jiang, G. S. and Shu, C. W., "Efficient Implementation of Weighted ENO Schemes," *Journal of Computational Physics*, Vol. 126, No. 1, 1996, pp. 202–228.

[25]Williamson, J., "Low-Storage Runge-Kutta Schemes," *Journal of Computational Physics*, Vol. 35, No. 1, 1980, pp. 48–56.

[26]Schrader, L. U., Brandt, L., and Henningson, D. S., "Receptivity Mechanisms in Three-Dimensional Boundary Layer Flows," *Journal of Fluid Mechanics*, Vol. 618, 2009, pp. 209–241.

[27]Choudhari, M. and Streett, C. L., "A Finite Reynolds-Number Approach for the Prediction of Boundary-Layer Receptivity in Localized Regions," *Phys. Fluids A*, Vol. 4, No. 11, 1992, pp. 2495–2514.

[28]Saric, W. S., West, D. E., Tufts, M. W., and Reed, H. L., "Flight Test Experiments on Discrete Roughness Element Technology for Laminar Flow Control," AIAA Paper 2015-0539, 2015.